INTERNATIONAL JOURNAL FOR NUMERICAL METHODS IN ENGINEERING, VOL. 39, 409–434 (1996)

NUMERICAL ANALYSIS OF SINGULARITIES IN TWO DIMENSIONS. PART 2: COMPUTATION OF GENERALIZED FLUX/STRESS INTENSITY FACTORS

BARNA A. SZABÓ AND ZOHAR YOSIBASH*

Center for Computational Mechanics, Washington University, Campus Box 1129, St. Louis, MO 63130, U.S.A.

SUMMARY

A numerical method for the computation of the generalized flux/stress intensity factors (GFIFs/GSIFs) for the asymptotic solution of linear second-order elliptic partial differential equations in two dimensions in the vicinity of singular points is described. Special attention is given to heat transfer and elasticity problems. The singularities may be caused by re-entrant corners and abrupt changes in material properties.

Such singularities are of great interest from the point of view of failure initiation: The eigenpairs, computed in a companion paper,[1] characterize the straining modes and their amplitudes (the GFIFs/GSIFs) quantify the amount of energy residing in particular straining modes. For this reason, failure theories directly or indirectly involve the GFIFs/GSIFs.

This paper addresses a general method based on the complementary weak formulation for determining the GFIFs/GSIFs numerically as a post-solution operation on the finite element solution vector. Importantly, the method is applicable to anisotropic materials, multi-material interfaces, and cases where the singularities are characterized by complex eigenpairs. An error analysis is sketched and numerical examples are presented to illustrate the effectiveness of the technique.

KEY WORDS: finite element methods; *p*-version; singular points; stress intensity factors; flux intensity factors; complementary energy; fracture mechanics; bi-material interfaces

1. INTRODUCTION

This is the second of two papers in which we discuss the computation of the solutions of linear elliptic partial differential equations, representing heat conduction or elastic deformation, in the vicinity of singular points. In the first paper,[1] numerical procedures were developed for computing the characteristic unknowns, called eigenpairs. The methods discussed in Reference 1, called the Steklov method and the modified Steklov method, are general, that is, applicable to singularities associated with corners and non-isotropic multi-material interfaces.

This paper presents a method for the extraction of the coefficients of the asymptotic expansion (GFIFs/GSIFs) once the eigenpairs are available. The stress intensity factors in the two-dimensional linear theory of elasticity are related to the amount of energy residing in the natural straining modes. They are, therefore, directly or indirectly connected with failure theories. We show in this paper that accurate computation of stress intensity factors (analogously flux intensity factors for heat transfer problems) is possible using a post-processing scheme over a small

* Present address: Dept. of Mechanical Engineering, Ben-Gurion University of the Negev, P.O. Box 653, Beer-Sheva 84105, Israel.

CCC 0029–5981/96/030409–26
© 1996 by John Wiley & Sons, Ltd.
Received 8 October 1994
Revised 18 April 1995

subdomain. It is shown that through utilization of the weak complementary formulation in conjunction with the modified Steklov method, and the *p*-version of the finite element method, the GFIFs/GSIFs can be computed with high accuracy for anisotropic as well as for isotropic domains.

Many methods exist for the extraction of stress intensity factors associated with *cracks* from finite element solutions. For example, the *J*-integral method, the energy release rate method, the stiffness derivative method, the contour integral method (CIM), the cutoff function method (CFM), the singular superelement method, etc. See for example References 2–5 and the references therein. Most of the methods, however, are applicable to crack singularities in isotropic materials only, and do not provide an arbitrary number of stress intensity factors.

One of the most efficient ways for extracting the GSIFs in a superconvergent manner is by CIM and CFM which are described in References 2 and 4. A variation of the CIM for the Laplace problem in three dimensions is presented in Reference 6, where mathematical analysis supported by numerical examples demonstrate that the flux intensity factors converge as fast as the energy, thus exhibit superconvergence. These efficient procedures use specially constructed extraction functions. These methods have three disadvantages: First, the CIM is not directly applicable to anisotropic multi-material interfaces because the eigenfunctions are not orthogonal with respect to the bilinear form. Second, a large number of extraction functions must be devised. Third, in the general elliptic problems the auxiliary functions are considerably less smooth, so that they cannot be approximated by the finite element method as well as the eigenfunctions corresponding to the positive eigenvalues.

The method presented in the following has the advantages of these superconvergent methods, without the drawbacks.

The outline of this paper is as follows. In Section 2 we demonstrate the method on the basis of the two-dimensional Laplace problem. This problem has been chosen because it is simple enough for demonstration purposes, yet contains all essential properties which are common to elliptic boundary value problems. The notations and the weak formulation for the extraction of the GFIFs is given. We also demonstrate that the method exhibits superconvergence. Numerical experiments are presented on the basis of a model problem, an L-shaped domain. In Section 3 the anisotropic heat transfer problem is discussed. The superconvergence property of the method is demonstrated through a numerical example. Section 4 is dedicated to elastostatic and problems involving cracks and complex eigenpairs. We present two numerical examples of a crack in an isotropic material, and a crack between two dissimilar materials, where complex eigenpairs appear.

2. GFIFS FOR THE LAPLACE PROBLEM—FORMULATION

The behaviour of the solution for the Laplace equation ($\nabla^2 u = 0$) in a two-dimensional domain in the vicinity of a singular point is best understood and is given by (see Reference 7):

$$u = \sum_{i=1}^{\infty} \sum_{s=0}^{S} \sum_{m=0}^{M} C_{ism} f_{ism}(\theta) r^{\alpha_i + m} \ln^s(r) \tag{1}$$

r and θ being the polar co-ordinates of a system located in the singular point. α_i are the eigenvalues (real numbers in case of the Laplace problem) and $f_{ism}(\theta)$ are the eigenfunctions which are analytical. Except for special cases, $S = 0$. M is either 0, or a positive integer when the boundary near the singular point (at the vertex) is curved. Note that the eigenpairs are uniquely determined by the geometry and material data.

When $\alpha_i < 1$, the corresponding ith term in the expansion (1) for ∇u is unbounded as $r \to 0$. We can think of the coefficients C_{ism} of these terms as analogous to the stress intensity factors of elasticity. We generalize this terminology, and refer to all coefficients C_{ism}, whether or not the corresponding terms in (1) are singular, as generalized flux intensity factors (GFIFs). The analogous coefficients in elasticity are called generalized stress intensity factors (GSIFs). The GSIFs are very important from the engineering point of view because they are related to failure theories.

Notation. Let Ω be a simply connected domain with boundaries $\partial\Omega = \bigcup_i \Gamma_i$ which are analytic simple arc curves called edges. These edges intersect at points called vertices. The Laplace problem $\nabla^2 u = 0$ is prescribed over Ω, with Dirichlet boundary conditions $u = \hat{u}$ on Γ^D and Neumann boundary conditions $du/dv = \hat{t}$ on $\partial\Omega - \Gamma_i^D$. Newton (also known as mixed) boundary conditions may be prescribed as well, but will not be considered here. Define the space $H_0^1(\Omega) = \{u \in H^1(\Omega) | u = 0 \text{ on } \Gamma_i^D\}$ where $H^1(\Omega)$ is the usual Sobolev space.

2.1. *The primal weak form*

In the primal formulation, the exact solution to the problem is defined by the weak form (the primal weak form):

$$\begin{aligned} &\text{Seek} \quad u \in H^1(\Omega), \quad u = \hat{u} \quad \text{on } \Gamma^D \text{ such that} \\ &\mathscr{B}(u, v) = \mathscr{F}(v) \quad \forall v \in H_0^1(\Omega) \end{aligned} \tag{2}$$

where the bilinear form is

$$\mathscr{B}(u, v) = \int_\Omega \sum_{i=1}^{2} \frac{\partial u}{\partial x_i} \frac{\partial v}{\partial x_i} \, d\Omega \tag{3}$$

and the linear form is

$$\mathscr{F}(v) = \int_{\partial\Omega - \Gamma^D} \hat{t} v \, ds \tag{4}$$

By $\|u\|_E = \sqrt{\mathscr{B}(u, u)}$ we denote the energy norm of u. Note that it is equivalent to the $H^1(\Omega)$ seminorm.

The exact solution u is analytic in Ω, except in the vicinity of the singular points (at the vertices), where the solution is given by the asymptotic expansion (1).

We use the p-version of the finite element method for approximating the solution of the weak form, i.e. we use a hierarchic sequence of finite element spaces $S_1(\Omega) \subset \cdots \subset S_i(\Omega) \subset H^1(\Omega)$. These finite element spaces consist of continuous piecewise polynomials of degree p on the elements of the mesh, such that the degree of the polynomial is increased as we go from S_i to S_{i+1}. Error estimation procedures in the energy norm for the p-version are summarized in Reference 8.

In the vicinity of the singular point P, see Figure 1, the exact solution u can be expanded as shown in (1) (we exclude for the moment the special cases where the $\ln r$ terms appear):

$$u = \sum_{i=1}^{\infty} A_i r^{\alpha_i} f_i(\theta) \tag{5}$$

In the case of the Laplace equation, α_i and $f_i(\theta)$ can be computed exactly using analytic methods, where in the general case numerical approximations are available using the modified Steklov method.

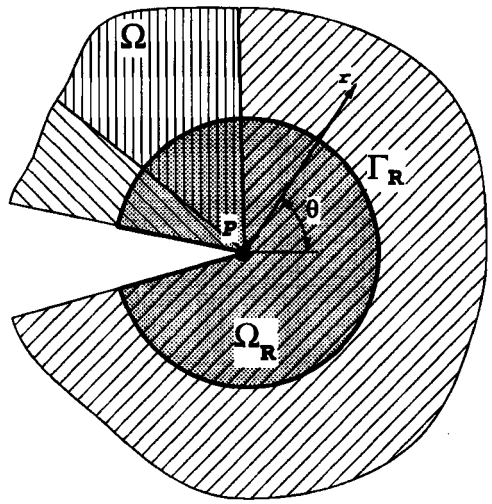

Figure 1. Typical singular point P

The following procedure is proposed: First we solve the problem over the entire domain Ω by means of the finite element method on the basis of the primal weak form (2), thus obtaining u_{FE}. Second, a small subdomain around the singular point is constructed. Define S_R as the interior points of a circle of radius R centred on the point P. The subdomain Ω_R is defined by $\Omega \cap S_R$ and its *circular* boundary is denoted by Γ_R. The flux vector is computed on S_R using (5).

For the complementary weak form the trial and test spaces are chosen to be linear combinations of the eigenfluxes, which are the derivatives of the eigenfunctions, after being obtained by the modified Steklov method,[1] *or analytically.*

The approximated finite element solution, u_{FE}, is applied on the boundary $\partial\Omega_R$ as the natural boundary conditions for the complementary problem. The finite element solution corresponding to the complementary weak form maximizes the complementary energy in Ω_R. Solving the finite element system of equation over Ω_R, one obtains an approximation for the series coefficients, the GFIFs.

2.2. *The complementary weak form*

We define the vector space $E_c(\Omega_R)$ as follows:

$$E_c(\Omega_R) = \left\{(q_x, q_y) \middle| \iint_{\Omega_R} |\mathbf{q}|^2 \, d\Omega < \infty, \frac{\partial q_x}{\partial x} + \frac{\partial q_y}{\partial y} = 0\right\} \tag{6}$$

We define by Γ_q that part of the boundary of Ω_R where Neumann boundary condition ($q_n = \hat{q}$) is prescribed. The space of admissible fluxes is denoted by $\tilde{E}_c(\Omega_R)$ and is defined by

$$\tilde{E}_c(\Omega_R) = \{(q_x, q_y) | (q_x, q_y) \in E_c(\Omega_R),\ q_n = \hat{q} \text{ on } \Gamma_q\} \tag{7}$$

Note that if $(q_x, q_y) = (\partial u/\partial x, \partial u/\partial y)$ then the condition $\partial q_x/\partial x + \partial q_y/\partial y = 0$ is the Laplace equation itself. The complementary weak form is stated as follows:

$$\begin{gathered} \text{Seek } \mathbf{q} \in \tilde{E}_c(\Omega_R) \quad \text{such that} \\ \mathscr{B}_c(\mathbf{q}, \mathbf{l}) = \mathscr{F}_c(\mathbf{l}) \quad \forall \mathbf{l} \in \tilde{E}_c(\Omega_R) \end{gathered} \tag{8}$$

where

$$\mathscr{B}_c(\mathbf{q}, \mathbf{l}) \equiv \iint_{\Omega_R} \mathbf{q} \cdot \mathbf{l} \, d\Omega = \iint_{\Omega_R} (q_x l_x + q_y l_y) r \, dr \, d\theta \tag{9}$$

and

$$\mathscr{F}_c(\mathbf{l}) \equiv \int_{\Gamma_g} \hat{u}(\mathbf{l} \cdot \mathbf{v}) \, ds = \int_{\Gamma_g} \hat{u}(l_x \cos\theta + l_y \sin\theta) \, ds \tag{10}$$

2.3. Sources of discretization errors

The extraction method described herein has three sources of discretization errors:

1. The fluxes are represented by a finite series of N terms. The exact representation is an infinite series.
2. The eigenpairs are only an approximation of the exact values (except when the exact solution is analytical). In the general case, therefore, we do not satisfy the condition of static admissibility exactly.
3. The boundary conditions are an approximation of the exact solution.

The first source of discretization error does not exist in the Laplace problem because the eigenpairs are orthogonal with respect to the bilinear form on Ω_R.

The second source of discretization error does not exist in case of the Laplace problem since the eigenpairs can be found analytically, thus do not have to be approximated. However, we shall demonstrate that an approximation of the eigenpairs (obtained by the modified Steklov method) is so accurate that the error is negligible for practical purposes.

2.4. GFIFs computation using the exact eigenpairs

First we describe the computation of the coefficients of the asymptotic expansion in the vicinity of a re-entrant corner using the exact eigenpairs. This eliminates the second source of discretization error. Consider, for example, a re-entrant corner of $(2\pi - \omega)$ degrees, where (q_x, q_y) are computed in terms of the *exact eigenpairs*:

$$\mathbf{q} = \begin{Bmatrix} \dfrac{\partial u}{\partial x} \\ \dfrac{\partial u}{\partial y} \end{Bmatrix} = \begin{Bmatrix} \cos\theta \dfrac{\partial u}{\partial r} - \dfrac{\sin\theta}{r} \dfrac{\partial u}{\partial \theta} \\ \sin\theta \dfrac{\partial u}{\partial r} + \dfrac{\cos\theta}{r} \dfrac{\partial u}{\partial \theta} \end{Bmatrix}, \quad 0 \leqslant \theta \leqslant \omega \tag{11}$$

where u is given for 'free–free' boundary conditions (i.e. $q_n = 0$ on the re-entrant straight boundaries) by

$$u = \sum_{n=0}^{\infty} A_n r^{\alpha_n} \cos(\alpha_n \theta), \quad \alpha_n \overset{\text{def}}{=} n\pi/\omega \tag{12}$$

therefore, (11) becomes

$$\mathbf{q} = \sum_{n=0}^{\infty} A_n \alpha_n r^{\alpha_n - 1} \begin{Bmatrix} \cos[(1 - \alpha_n)\theta] \\ \sin[(1 - \alpha_n)\theta] \end{Bmatrix} \tag{13}$$

The elements of the compliance matrix $[B_c]$, which correspond to the bilinear form $\mathscr{B}_c(\mathbf{q}, \mathbf{l})$, are given by

$$(B_c)_{ij} = \int_0^R \int_0^\omega \alpha_i \alpha_j r^{\alpha_i + \alpha_j - 1} \cos[(\alpha_j - \alpha_i)\theta] \, dr \, d\theta \tag{14}$$

Finally, after integrating, we have the following:

$$(B_c)_{ij} = \begin{cases} 0, & i \neq j \\ (\alpha_i/2) R^{2\alpha_i} \omega, & i = j \end{cases} \tag{15}$$

Consider now the expression for the linear form $\mathscr{F}_c$. This can be divided into two terms: One corresponding to the circular boundary called Γ_3, the other corresponding to the straight boundaries Γ_1 and Γ_2 which intersect in the singular point.

Assume that the solution on Γ_3 is given by $u|_{\Gamma_3} = \hat{u}(\theta)$:

$$(\mathscr{F}_c^{\Gamma_3})(\mathbf{l}) = \int_{\Gamma_3} \hat{u}(\theta)(l_x \cos\theta + l_y \sin\theta) R \, d\theta \tag{16}$$

After substituting $\mathbf{l}$, which is in the form (13), (16) becomes

$$(\mathscr{F}_c^{\Gamma_3})(\mathbf{l}) = \sum_{n=0}^{\infty} B_n \alpha_n R^{\alpha_n} \int_0^\omega \cos(\alpha_n \theta) \hat{u}(\theta) \, d\theta \tag{17}$$

The elements of the load vector $\{F_c^{\Gamma_3}\}$, which correspond to the linear form $(\mathscr{F}_c^{\Gamma_3})(\mathbf{l})$ can be evaluated explicitly:

$$(F_c^{\Gamma_3})_i = \alpha_i R^{\alpha_i} \int_0^\omega \cos(\alpha_i \theta) \hat{u}(\theta) \, d\theta \tag{18}$$

For the case of 'free–free' boundary condition, $q_n = 0$ on Γ_1 and Γ_2. This condition, in the framework of the maximum complementary energy formulation, has to be treated by constraining the admissible trial function field. However, by using the exact eigenpairs in constructing the trial space, the constraints are automatically satisfied because the chosen $\mathbf{q}$ in (13) satisfies the condition $q_n = 0$ on Γ_1 and Γ_2.

The 'fixed–free', 'fixed–fixed' and 'free–fixed' boundary conditions are treated analogously.

Theorem 1. The error in the load vector due to replacing u_{EX} with u_{FE} is bounded by the error in energy norm. $F_c(e) \leqslant C(R) \| e \|_E$.

The proof can be found in Reference 9.

Remark 1. When the compliance matrix is formulated using the exact eigenpairs, no discretization errors are associated with the compliance matrix of the complementary weak form. Because the compliance matrix is diagonal (equation (15)), we conclude that the convergence rate of the GFIFs and first derivatives at internal points is at least as fast as the energy norm.

Numerical examples presented in Reference 9 indicate that errors in the computed GFIFs converge much faster than the error in energy norm, in fact, as fast as the errors in the strain energy. It is also shown in Reference 9 that the formula used for computing flux intensity factors is identical to the one obtained using the contour integral method which is known to be superconvergent for the Laplace problem.

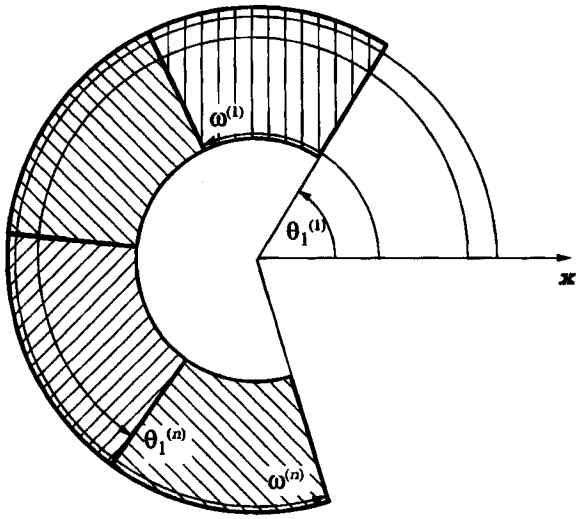

Figure 2. Notation

2.5. *GFIFs computation using the approximated eigenpairs*

In general scalar elliptic problems the exact eigenpairs are not known. The modified Steklov method is employed for computing the eigenpairs. The domain of application of the modified Steklov method is the annular sector shown in Figure 2. The finite element solution, u_{FE}, can be represented by the linear combinations of the eigenfunctions:

$$u_{FE} = \sum_{j=1}^{\infty} \hat{A}_j r^{\hat{\alpha}_j} \hat{f}_j(\theta) \tag{19}$$

where $\hat{f}_j(\theta)$ are piecewise polynomials. Specifically, referring to Figure 2, on the kth material segment we have the linear mapping:

$$\theta(\xi) = \frac{\omega^{(k)} + \theta_1^{(k)}}{2} + \frac{\omega^{(k)} - \theta_1^{(k)}}{2}\xi, \quad -1 \leqslant \xi \leqslant 1$$

and

$$\hat{f}_j(\theta(\xi)) = \sum_{i=1}^{p+1} c_{ij}^{(k)} N_i(\xi), \quad k = 1, 2, \ldots, n$$

where $N_i(\xi)$ are the hierarchic shape functions for one-dimensional elements described in Reference 10, and n is the number of partitions used for computing the approximated eigenpairs.

The modified Steklov method solved by the finite element method ensures the convergence of the eigenpairs with respect to increasing degrees of freedom (DOF):

$$\lim_{\text{DOF}\to\infty} (\hat{\alpha}_j, \hat{f}_j(\theta)) = (\alpha_j, f_j(\theta)) \tag{20}$$

so that the flux vector computed from the approximated eigenpairs, in the limit, belongs to the space $\tilde{E}_c(\Omega_R)$. It is not difficult to show that the resulting flux vectors are square integrable.

In the following we formulate the complementary weak form for the case where the eigenpairs are only an approximation of the exact values. These approximations are obtained using the modified Steklov method reported in Reference 1, where we show that an excellent approximation can be achieved with a small effort. We examine this case since in general scalar elliptic problems, including the elasticity problems, the eigenpairs cannot by computed analytically for general singular points when the materials are anisotropic.

We now formulate the variational formulation explicitly. Based on (19), we obtain

$$\begin{Bmatrix} q_x \\ q_y \end{Bmatrix} = \sum_{j=1}^{\infty} \hat{A}_j r^{\hat{\alpha}_j - 1} \begin{Bmatrix} \sum_{i=1}^{p+1} c_{ij}^{(k)} \left(\hat{\alpha}_j N_i(\xi) \cos\theta - \dfrac{\omega^{(k)} - \theta_1^{(k)}}{2} \dfrac{\mathrm{d}N_i(\xi)}{\mathrm{d}\xi} \sin\theta \right) \\ \sum_{i=1}^{p+1} c_{ij}^{(k)} \left(\hat{\alpha}_j N_i(\xi) \sin\theta + \dfrac{\omega^{(k)} - \theta_1^{(k)}}{2} \dfrac{\mathrm{d}N_i(\xi)}{\mathrm{d}\xi} \cos\theta \right) \end{Bmatrix} \tag{21}$$

The expression for the complementary bilinear form is based on (9), and after substituting (21) we obtain

$$\begin{aligned} \mathscr{B}_c(\mathbf{q}, \mathbf{q}) &= \int_{\theta_1}^{\omega} \int_0^R (q_x^2 + q_y^2) r \, \mathrm{d}r \, \mathrm{d}\theta \\ &= \sum_{j,\ell=1}^{N} \hat{A}_j \hat{A}_\ell \frac{R^{\hat{\alpha}_j + \hat{\alpha}_\ell}}{(\hat{\alpha}_j + \hat{\alpha}_\ell)} \sum_{i,k=1}^{p+1} \int_{\theta_1}^{\omega} [\hat{\alpha}_j \hat{\alpha}_\ell N_i N_k + N_i' N_k'] c_{ij} c_{k\ell} \, \mathrm{d}\theta \end{aligned} \tag{22}$$

N being the number of eigenpairs used in (21) (instead of infinity), and $\theta_1^{(1)} \equiv \theta_1$, $\omega^{(n)} \equiv \omega$.

Assume that the finite element mesh used for computing the eigenpairs has n elements in the circumferential direction and a polynomial degree p. Using a Gauss quadrature of N_G points, the explicit expression for each term in the compliance matrix is given by

$$\begin{aligned} (B_c)_{ij} = \frac{R^{\hat{\alpha}_i + \hat{\alpha}_j}}{(\hat{\alpha}_i + \hat{\alpha}_j)} \sum_{l=1}^{n} \hat{\alpha}_i \hat{\alpha}_j \sum_{k,\ell=1}^{p+1} c_{ik}^{(l)} c_{j\ell}^{(l)} \Bigg[\left(\frac{\omega^{(l)} - \theta_1^{(l)}}{2} \sum_{m=1}^{N_G} W_m N_k(\xi_m) N_\ell(\xi_m) \right) \\ + \left(\frac{2}{\omega^{(l)} - \theta_1^{(l)}} \sum_{m=1}^{N_G} W_m N_k'(\xi_m) N_\ell'(\xi_m) \right) \Bigg] \end{aligned} \tag{23}$$

where W_m and ξ_m are the weights and abscissas of the Gauss quadrature and n is the number of partitions used for computing the approximated eigenpairs (see Reference 11 for details).

Remark 2. If the exact eigenfunctions were used then we would have $(B_c)_{ij} = c_i \delta_{ij}$, therefore only the diagonal terms would have to be computed. The values $(B_c)_{ij}$, $i \neq j$, are computed to assess the accuracy of the approximated eigenpairs.

We proceed now to the evaluation of the linear form corresponding to the principle of maximum complementary energy. Consider first the term corresponding to Γ_3.

Substituting (21) in (10) the linear form corresponding to Γ_3 becomes

$$\mathscr{F}_c^{\Gamma_3}(\mathbf{q}) = \sum_{l=1}^{n} \int_{\theta_1^{(l)}}^{\omega^{(l)}} \hat{u}(\theta) \left[\sum_{j=1}^{N} \hat{A}_j \hat{\alpha}_j R^{\hat{\alpha}_j} \sum_{i=1}^{p+1} c_{ij}^{(l)} N_i(\theta(\xi)) \right] \mathrm{d}\theta \tag{24}$$

The explicit expression for each term in the load vector is given by

$$(F_c)_i = \hat{\alpha}_i R^{\hat{\alpha}_i} \sum_{l=1}^{n} \sum_{k=1}^{p+1} c_{ik}^{(l)} \frac{\omega^{(l)} - \theta_1^{(l)}}{2} \sum_{m=1}^{N_G} W_m N_k(\xi_m) \hat{u}(\theta(\xi_m)) \tag{25}$$

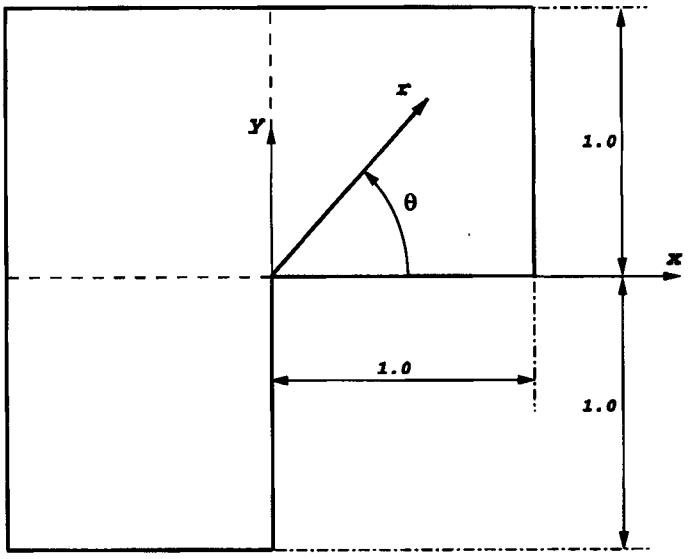

Figure 3. The L-shaped example problem and the finite element mesh

The boundary conditions on Γ_1 and Γ_2 are fulfilled automatically because the approximated eigenpairs satisfy them.

Note that the finite element discretization over the domain Ω may be different from the one used for the modified Steklov problem.

2.6. *Numerical example*

The example discussed in this section is constructed so that the exact solution is known. It demonstrates: (a) the influence of the approximated eigenpairs, obtained using the modified Steklov method, on the accuracy of the extracted GFIFs and (b) the performance and efficiency of the proposed extraction method.

We consider a 90° V-notch in an infinite domain. We 'remove' the L-shaped domain shown in Figure 3, and impose on its boundaries the Neumann boundary conditions corresponding to the exact analytic solution, which is known. The exact asymptotic solution for this free–free V-notch is given by (12) and the derivatives in x and y directions (q_x, q_y) to be imposed on the boundaries of the L-shaped domain are given by (13).

First, an approximation to the eigenpairs has to be obtained. The modified Steklov method is used over a mesh containing two elements shown in Figure 4. As the p-level of the shape functions is increased over the mesh in Figure 4, a better approximation of the eigenpairs is obtained. We will use the eigenpairs obtained when assigning p-levels 4, 5, 6, 7 and 8 for the computation of the approximated GFIFs.

Once the approximated eigenpairs are available, a finite element solution is sought for the L-shaped domain. We construct a mesh containing the minimum possible number of elements over the L-shaped domain without any refinements in the vicinity of the singular point, as shown in Figure 3. The boundary conditions in (13) were imposed on the L-shaped boundaries, with the GFIFs chosen to be: $A_1 = 1$, $A_2 = \frac{1}{2}$, $A_3 = \frac{1}{3}$, $A_4 = \frac{1}{4}$, $A_5 = \frac{1}{5}$ and $A_i = 0$ $(i = 6, 7, \ldots)$. The GFIFs were then extracted using the proposed method, taking R to be 0·9. The results of

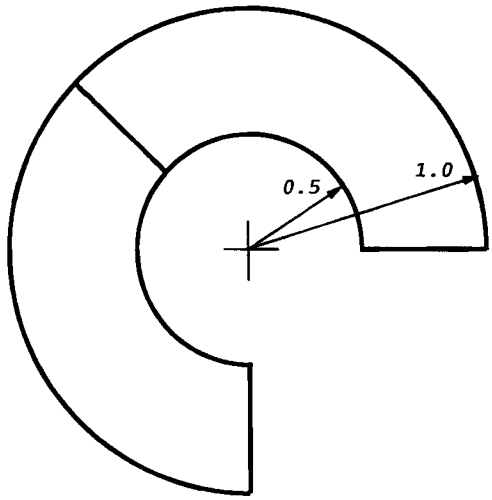

Figure 4. Mesh for the computation of the approximated eigenpairs

these computations are displayed in Table I. The following conclusions may be drawn from the results shown in Table I:

1. The errors in the approximated ith eigenpair do not influence the accuracy of the jth GFIF. This is because the eigenfunctions are orthogonal.
2. The error in the GFIFs is always bounded by the error in energy norm when the error in the eigenpairs is less than 0·1 per cent. Moreover, in this case the error in the GFIFs is virtually the same as if the exact eigenvalues had been used to extract the GFIFs.
3. Using the coarsest mesh possible for the extraction of both the eigenpairs and the GFIFs, excellent results have been obtained. The relative error in the first five eigenpairs is less than 0·007 per cent, and the relative error in the first five GFIFs is less than 0·7 per cent when the relative error in energy norm is 2·6 per cent.

3. EXTRACTION OF GFIFS FOR THE GENERAL SCALAR ELLIPTIC PROBLEM

In the following it is shown that extraction of GFIFs for the general scalar elliptic problem

$$\frac{\partial}{\partial x_1}\left(a_{11}\frac{\partial u}{\partial x_1}+a_{12}\frac{\partial u}{\partial x_2}\right)+\frac{\partial}{\partial x_2}\left(a_{21}\frac{\partial u}{\partial x_1}+a_{22}\frac{\partial u}{\partial x_2}\right)=0$$

is possible by utilizing the same methods as for the Laplace problem. In the general case the eigenfunctions are not orthogonal with respect to the bilinear form, and therefore the compliance matrix becomes fully populated. Nevertheless, the eigenfunctions remain linearly independent, so that the GFIFs can be computed using the complementary weak form.

We start our discussion by formulating the principle of maximum complementary energy for the general scalar elliptic problem (we assume that in the neighbourhood of the singular point $a_{ij}=a_{ij}(\theta)$ and $a_{12}=a_{21}$). The weak form is stated exactly as in (8), except that the bilinear and

Table I. Relative error (%) in computed GFIFs for the L-shaped domain

p-level for eigenvalue computation	GFIF #	Error in eigenvalue (%)	$p=4$	$p=5$	$p=6$	$p=7$	$p=8$	Extrapolated
$p=4$	$\hat{A}_1$	0·0002	−1·63	−0·75	−0·38	−0·45	−0·31	−0·5
	$\hat{A}_2$	0·03	0·54	0·36	0·36	0·42	0·41	0·4
	$\hat{A}_3$	0·39	6·79	6·84	6·87	6·87	6·84	6·87
	$\hat{A}_4$	0·73	7·12	7·68	7·64	7·52	7·56	7·56
	$\hat{A}_5$	17	28·5	25·55	26·15	34·4	26·8	26·85
$p=5$	$\hat{A}_1$	3×10^{-6}	−1·62	−0·73	−0·36	−0·43	−0·30	−0·48
	$\hat{A}_2$	3×10^{-5}	0·12	−0·064	−0·064	0·001	−0·0096	−0·016
	$\hat{A}_3$	0·035	0·54	0·63	0·61	0·61	0·61	0·62
	$\hat{A}_4$	0·71	7·2	7·76	7·72	7·6	7·64	7·6
	$\hat{A}_5$	2·4	29·5	26·65	27·5	28·7	28·1	28·35
$p=6$	$\hat{A}_1$	$4{\cdot}5\times10^{-8}$	−1·62	−0·73	−0·37	−0·43	−0·29	−0·48
	$\hat{A}_2$	$2{\cdot}25\times10^{-5}$	0·122	−0·058	−0·058	0·0066	−0·0044	−0·01
	$\hat{A}_3$	0·0018	−0·216	−0·135	−0·138	−0·160	−0·17	−0·147
	$\hat{A}_4$	0·0084	−0·52	0·009	−0·044	−0·136	−0·112	−0·116
	$\hat{A}_5$	0·49	6·2	3·6	4·19	5·05	4·69	4·77
$p=7$	$\hat{A}_1$	$<10^{-9}$	−1·62	−0·73	−0·37	−0·43	−0·29	−0·48
	$\hat{A}_2$	3×10^{-8}	0·13	−0·05	−0·05	−0·016	0·005	−0·001
	$\hat{A}_3$	$7{\cdot}8\times10^{-5}$	−0·08	−0·01	−0·0048	−0·027	−0·037	−0·037
	$\hat{A}_4$	0·0069	−0·71	−0·184	−0·235	−0·326	−0·302	−0·304
	$\hat{A}_5$	0·063	1·235	−1·235	−0·639	−0·212	−0·173	−0·0825
$p=8$	$\hat{A}_1$	$<10^{-9}$	−1·62	−0·73	−0·37	−0·43	−0·30	−0·48
	$\hat{A}_2$	$<10^{-9}$	0·13	−0·05	−0·05	0·016	0·0046	−0·0015
	$\hat{A}_3$	$2{\cdot}3\times10^{-6}$	−0·058	0·021	0·027	0·004	−0·0055	0·009
	$\hat{A}_4$	$3{\cdot}7\times10^{-5}$	−0·427	0·099	0·047	−0·044	−0·021	−0·022
	$\hat{A}_5$	0·0064	2·07	−0·436	0·155	1·0	0·63	0·715
$p=\infty$	$\hat{A}_1$	0	−1·63	−0·73	−0·36	−0·43	−0·30	−0·48
	$\hat{A}_2$	0	−1·34	−0·05	−0·05	−0·014	−0·004	−0·016
	$\hat{A}_3$	0	0	0	0	0	0	0
	$\hat{A}_4$	0	−0·41	0·108	0·056	−0·03	−0·0096	−0·011
	$\hat{A}_5$	0	1·5	−0·92	−0·33	0·49	0·105	0·207
Relative error in energy norm $\|e\|_E$ (%)			6·02	4·65	3·74	3·10	2·62	

linear forms are as follows:

$$\begin{aligned}\mathscr{B}_c(\mathbf{q},\mathbf{l}) &\equiv \int\int_{\Omega_R} (\mathbf{q})^T \begin{bmatrix} a_{11} & a_{12} \\ a_{21} & a_{22} \end{bmatrix} \mathbf{l}\, d\Omega \\ &= \int_0^R \int_{\theta_1}^{\omega} \sum_{i,j=1}^{2} a_{ij} \frac{\partial u}{\partial x_i}\frac{\partial v}{\partial x_j} r\, dr\, d\theta \\ &= \int_0^R \int_{\theta_1}^{\omega} (a_{11}\cos^2\theta + a_{12}\sin 2\theta + a_{22}\sin^2\theta)\frac{\partial u}{\partial r}\frac{\partial v}{\partial r} \\ &\quad + (a_{11}\sin^2\theta - a_{12}\sin 2\theta + a_{22}\cos^2\theta)\frac{1}{r^2}\frac{\partial u}{\partial \theta}\frac{\partial v}{\partial \theta} \\ &\quad + (\tfrac{1}{2}(a_{22}-a_{11})\sin 2\theta + a_{12}\cos 2\theta)\frac{1}{r}\left(\frac{\partial u}{\partial \theta}\frac{\partial v}{\partial r} + \frac{\partial u}{\partial r}\frac{\partial v}{\partial \theta}\right) r\, dr\, d\theta \end{aligned} \tag{26}$$

$$\mathscr{F}_c(\mathbf{I}) \equiv \int_{\Gamma_u} \hat{u}(\mathbf{l}\cdot\mathbf{v})\,ds = \int_{\Gamma_u} \hat{u} \sum_{i,j=1}^{2} a_{ij}\frac{\partial v}{\partial x_i} v_j\,ds$$

$$= R\int_{\theta_1}^{\omega} [\hat{u}]_R \Bigg[(a_{11}\cos^2\theta + a_{12}\sin 2\theta + a_{22}\sin^2\theta)\frac{\partial v}{\partial r}$$

$$+ (\tfrac{1}{2}(a_{22} - a_{11})\sin 2\theta + a_{12}\cos 2\theta)\frac{1}{R}\frac{\partial v}{\partial \theta}\Bigg]_R d\theta \tag{27}$$

where we assumed that the domain Ω_R is defined as in Section 2, i.e. a circular sector, and the vector $\mathbf{q}$ (resp. $\mathbf{l}$) is related to u (resp. v) by equation (11).

The ith eigen-combination is denoted by $\Phi_i(\alpha_i, r, \theta)$:

$$\Phi_i(\alpha_i, r, \theta) = r^{\alpha_i} f_i(\theta) \tag{28}$$

Any two of Φ_i and Φ_j are linearly independent, however unlike in the case of the Laplace problem, they are not orthogonal with respect to the bilinear form $\mathscr{B}_c$ on a *circular sector domain* Ω_R centred in the singular point with a radius R.

Theorem 2. In case of the general scalar elliptic problem the eigenfunctions $f_i(\theta)$ are no longer orthogonal with respect to $\mathscr{B}_c$ *over* Ω_R.

The proof can be found in Reference 11.

Remark 3. The lack of orthogonality in the general elliptic scalar problem complicates considerably the use of the CIM for the extraction of the GFIFs, requiring the use an orthogonalization procedure.

3.1. Extraction procedures in the vicinity of singular points

Following the same steps as in previous section, the (i, j)th term of the compliance matrix is given by

$$(B_c)_{ij} = \frac{R^{\alpha_i+\alpha_j}}{(\alpha_i+\alpha_j)} \sum_{l=1}^{n} \sum_{k,\ell=1}^{p+1} \sum_{m=1}^{N_G} W_m c_{ik}^{(l)} c_{j\ell}^{(l)}$$

$$\times \Bigg\{ \frac{\omega^{(l)} - \theta_1^{(l)}}{2} \alpha_i\alpha_j (a_{11}^{(l)}\cos^2[\theta(\xi_m)] + a_{12}^{(l)}\sin[2\theta(\xi_m)] + a_{22}^{(l)}\sin^2[\theta(\xi_m)]) N_k(\xi_m) N_\ell(\xi_m)$$

$$+ \frac{2}{\omega^{(l)} - \theta_1^{(l)}} (a_{11}^{(l)}\sin^2[\theta(\xi_m)] - a_{12}^{(l)}\sin[2\theta(\xi_m)] + a_{22}^{(l)}\cos^2[\theta(\xi_m)]) N_k'(\xi_m) N_\ell'(\xi_m)$$

$$+ (\tfrac{1}{2}(a_{22}^{(l)} - a_{11}^{(l)})\sin[2\theta(\xi_m)] + a_{12}^{(l)}\cos[2\theta(\xi_m)])(\alpha_i N_k(\xi_m) N_\ell'(\xi_m) + \alpha_j N_k'(\xi_m) N_\ell(\xi_m)) \Bigg\} \tag{29}$$

and the i-term of the linear form is

$$(F_c)_i = R^{\alpha_i} \sum_{l=1}^{n} \sum_{k=1}^{p+1} \sum_{m=1}^{N_G} \hat{u}(\theta(\xi_m)) W_m c_{ik}^{(l)}$$
$$\times \left[\alpha_i \frac{\omega^{(l)} - \theta_1^{(l)}}{2} (a_{11}^{(l)} \cos^2[\theta(\xi_m)] + a_{12}^{(l)} \sin[2\theta(\xi_m)] + a_{22}^{(l)} \sin^2[\theta(\xi_m)]) N_k(\xi_m) \right.$$
$$\left. + (\tfrac{1}{2}(a_{22}^{(l)} - a_{11}^{(l)}) \sin[2\theta(\xi_m)] + a_{12}^{(l)} \cos[2\theta(\xi_m)]) N_k'(\xi_m) \right] \tag{30}$$

The computation of the matrix B_c involves only the eigenpairs. The computation of the vector F_c involves the eigenpairs and the solution $\hat{u}$ given on a circle of radius R around the singular point.

3.2. *Model problem*

Consider the general scalar elliptic problem governed by the equation:

$$a_{11} \frac{\partial^2 u}{\partial x_1^2} + a_{22} \frac{\partial^2 u}{\partial x_2^2} = 0, \quad a_{11} = 4, \; a_{22} = 1 \tag{31}$$

prescribed over a domain Ω whose boundary consists of a reentrant corner of 90° generated by two edges, Γ_1 and Γ_2. On the two edges Γ_1 and Γ_2, which meet at the origin of the co-ordinate system (x_1, x_2), homogeneous Neumann boundary conditions are applied:

$$\sum_{i,j=1}^{2} a_{ij} \frac{\partial u}{\partial x_i} \nu_j = 0 \quad \text{on } \Gamma_1, \Gamma_2 \tag{32}$$

The solution u can be written in the following form:

$$u = \sum_{n=1}^{\infty} A_n u^{(n)} + \text{constant} \tag{33}$$

where

$$u^{(n)} = r^{2n/3} 2^{-2n/3} (1 + 3\sin^2\theta)^{n/3} \cos\left[\frac{2n}{3} \arctan(2\tan\theta) \right] \tag{34}$$

r and θ are polar co-ordinates centred on the re-entrant corner such that $\theta = 0$ coincides with the x axis. The first term in the expansion (33) for ∇u is unbounded as $r \to 0$.

Let Ω be the unit circle sector shown in Figure 5, which is divided into six finite elements, such that the refined finite element layer around the singular point has the radius 0·15. The circular boundary of the domain is loaded by the Neumann boundary condition which corresponds to the first symmetric eigenfunction of the asymptotic expansion of u about the reentrant corner:

$$q_\nu = (a_{11}\cos^2\theta + a_{22}\sin^2\theta) \frac{\partial u}{\partial r} + \tfrac{1}{2}\sin 2\theta (a_{22} - a_{11}) \left(\frac{1}{r} \frac{\partial u}{\partial \theta} \right)$$
$$= A_1 r^{-1/3} [2(1 + 3\sin^2\theta)]^{-2/3} \{ [\tfrac{2}{3}(1 + 3\cos^2\theta)(1 + 3\sin^2\theta) - \tfrac{3}{2}\sin^2 2\theta]$$
$$\times \cos[\tfrac{2}{3}\arctan(2\tan\theta)] + 2\sin 2\theta \sin[\tfrac{2}{3}\arctan(2\tan\theta)] \} \tag{35}$$

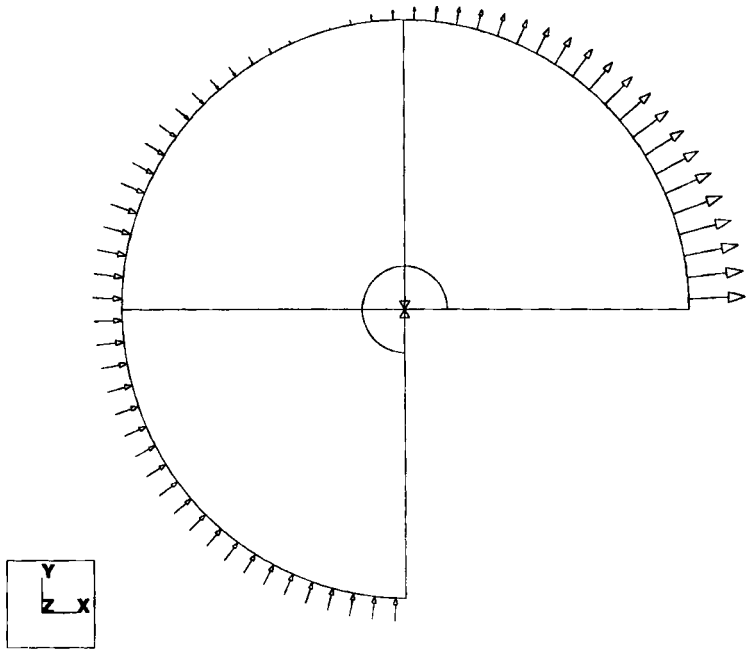

Figure 5. Solution domain, mesh design (six elements), and flux boundary conditions for the model problem

Table II. First three GFIFs for the model problem with 6-element mesh

	$p=1$	$p=2$	$p=3$	$p=4$	$p=5$	$p=6$	$p=7$	$p=8$
DOF	8	22	39	62	91	126	167	214
$\|e\|_E$(%)	33·95	7·02	3·74	2·23	1·65	1·32	1·10	0·93
A_1	0·8027116	0·9905142	0·9997004	0·9997054	0·9993824	0·9995902	0·9997769	0·9998464
A_2	0·1694275	0·0038147	0·0036318	$2{\cdot}38\times10^{-4}$	$1{\cdot}5\times10^{-4}$	$7{\cdot}8\times10^{-5}$	$4{\cdot}6\times10^{-5}$	$3{\cdot}4\times10^{-5}$
A_3	1×10^{-10}	5×10^{-10}	4×10^{-10}	5×10^{-10}	5×10^{-10}	5×10^{-10}	5×10^{-10}	5×10^{-10}

while on the other two boundaries homogeneous Neumann boundary conditions are applied. The GFIF A_1 is arbitrarily selected to be $A_1 = 1$.

To demonstrate the entire numerical procedure, we do not use the exact eigenpairs in our computations but their approximations obtained by the modified Steklov method. These eigenpairs are computed using a coarse 3-element mesh. The first three approximated eigenvalues obtained at $p = 8$ are $\alpha_1 = 0{\cdot}666666675$, $\alpha_2 = 1{\cdot}333333307$ and $\alpha_3 = 2{\cdot}000000413$.

The first three GFIFs were then extracted, taking R to be 0·5. The number of degrees of freedom, the error in energy norm, and the computed values of the three GFIFs are listed in Table II. Of course, A_1 has to converge to 1, and A_2 and A_3 have to converge to 0.

We may see from Table II that the GFIFs converge strongly and obviously, although not monotonically. Our method yields solutions at p-level 2 or 3 that are within the range of precision normally needed in engineering computations.

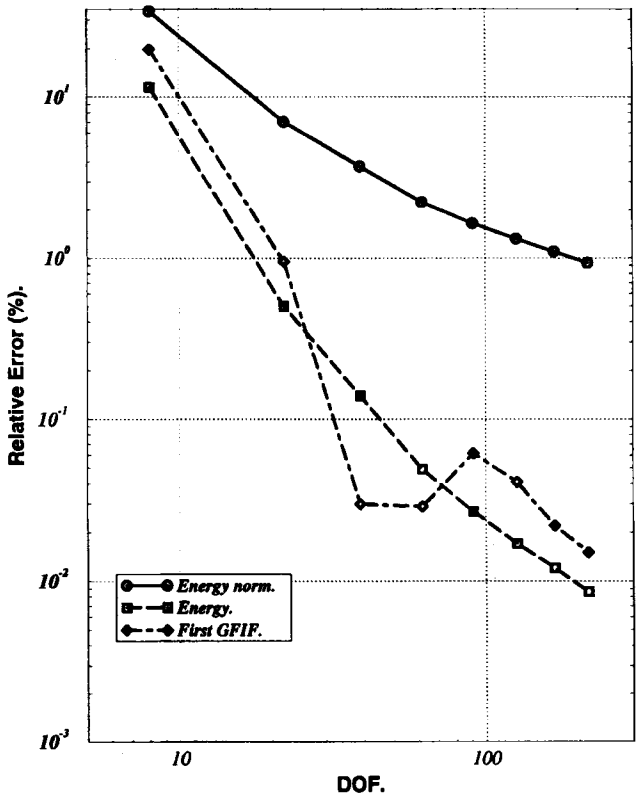

Figure 6. Convergence of $\|e\|_E$, the strain energy ($\|e\|_E^2$), and A_1 for the 6-element mesh

We have plotted the relative error in energy norm, the relative error in strain energy and the absolute value of the relative error in A_1 on a log–log scale in Figure 6.

The convergence path of the GFIF A_1 follows closely that of the strain energy, which is a behaviour referred to as 'superconvergence'.

Taking advantage of the strong convergence observed, we use now over the same domain only three finite elements, without the refined layer towards the singular point. The integration path was taken to be $R = 0{\cdot}9$, and we plot the same data as in Figure 6 for the 3-element mesh in Figure 7. The convergence curve of the GFIF A_1 is oscillating with a mean being approximately the strain energy convergence curve.

This anisotropic model problem clearly demonstrates the effectiveness and the superconvergent property of the proposed method for anisotropic materials.

4. GSIFS FOR THE ELASTOSTATIC PROBLEM

This section is devoted to the computation of the generalized stress intensity factors associated with the elastostatic problem. Although the basic method has already been presented in the previous two sections, new difficulties arise because of the existence of complex eigenpairs.

As shown in Reference 11, when one of the eigenpairs is complex then both the real and the imaginary part of the solution must be considered. Assume that the jth eigenpair is complex,

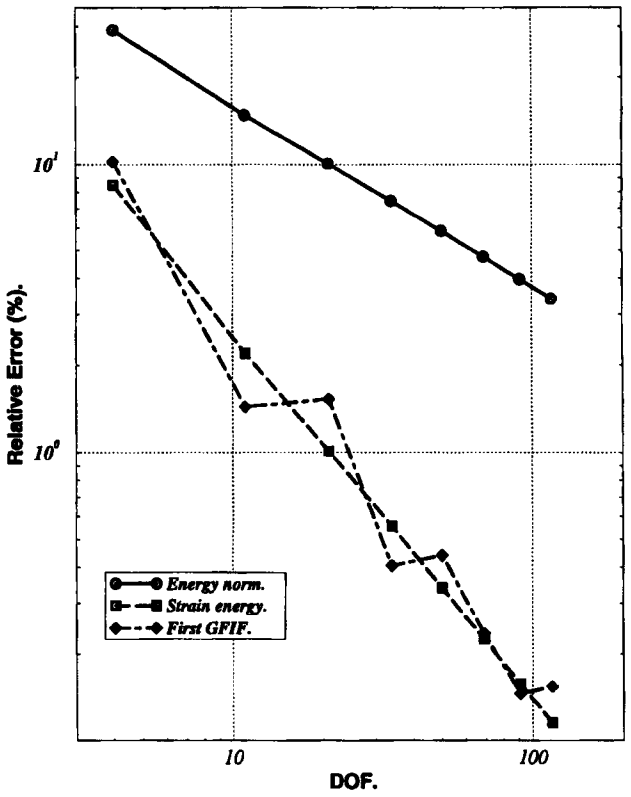

Figure 7. Convergence of $\|e\|_E$, the strain energy ($\|e\|_E^2$), and A_1 for the 3-element mesh

i.e. $\alpha_j = \alpha_j^{(\mathscr{R})} + i\alpha_j^{(\mathscr{I})}$ and the corresponding complex eigenvector associated with u_x is $\{\mathbf{a}_j\} = \{\mathbf{a}_j^{(\mathscr{R})} + i\mathbf{a}_j^{(\mathscr{I})}\}$, while the one associated with u_y is $\{\mathbf{b}_j\} = \{\mathbf{b}_j^{(\mathscr{R})} + i\mathbf{b}_j^{(\mathscr{I})}\}$. We need to consider both the real and the imaginary parts of the solution, i.e. the span of the space in which the solution lies contains the two eigenfunctions corresponding to the real and imaginary parts:

$$\begin{Bmatrix} u_x \\ u_y \end{Bmatrix}_j = r^{\alpha_j^{(\mathscr{R})}} \sum_{m=1}^{p+1} \begin{Bmatrix} a_{jm}^{(\mathscr{R})} \cos(\alpha_j^{(\mathscr{I})} \ln r) - a_{jm}^{(\mathscr{I})} \sin(\alpha_j^{(\mathscr{I})} \ln r) \\ b_{jm}^{(\mathscr{R})} \cos(\alpha_j^{(\mathscr{I})} \ln r) - b_{jm}^{(\mathscr{I})} \sin(\alpha_j^{(\mathscr{I})} \ln r) \end{Bmatrix} N_m(\xi)$$

$$\begin{Bmatrix} u_x \\ u_y \end{Bmatrix}_{j+1} = r^{\alpha_j^{(\mathscr{R})}} \sum_{m=1}^{p+1} \begin{Bmatrix} a_{jm}^{(\mathscr{R})} \sin(\alpha_j^{(\mathscr{I})} \ln r) - a_{jm}^{(\mathscr{I})} \cos(\alpha_j^{(\mathscr{I})} \ln r) \\ b_{jm}^{(\mathscr{R})} \sin(\alpha_j^{(\mathscr{I})} \ln r) - b_{jm}^{(\mathscr{I})} \cos(\alpha_j^{(\mathscr{I})} \ln r) \end{Bmatrix} N_m(\xi) \tag{36}$$

When the jth eigenvalue is real, then the second eigenfunction vector vanishes, and the only eigenfunction vector corresponding to the jth eigenvalue is:

$$\begin{Bmatrix} u_x \\ u_y \end{Bmatrix}_j = r^{\alpha_j} \sum_{m=1}^{p+1} \begin{Bmatrix} a_{jm} \\ b_{jm} \end{Bmatrix} N_m(\xi)$$

Once the solution is given in terms of the eigenpairs, the expressions for the bilinear form ($\mathscr{B}_c$) and the linear form ($\mathscr{F}_c$) associated with the complementary weak form can be evaluated.

Before doing so, we examine an interesting feature of the stress intensity factors (K_I and K_{II}) for crack configurations in cases when the first eigenvalue is complex. It was shown in 1959 by Williams[12] that the stresses near the crack tip have an oscillatory character as $r \to 0$. Therefore, the linear solution is physically inadmissible because it predicts that the upper and lower surfaces of the crack should wrinkle and overlap near the ends of the crack. Nevertheless, the size regions in which overlapping occur is significantly smaller when compared with crack size for actual materials (see for example References 13 and 14). This region can be neglected in a similar manner as the plastic zone, when failure theorems based on linear fracture mechanics are applied. Moreover, the stress intensity factors do not have the simple physical interpretation, as in the homogeneous case, where the symmetric and skew-symmetric parts of the solution appear separately. Hence, in the formulation of failure criteria, it is necessary to assume that some function of K_I and K_{II} (and, possibly, additional GSIFs), has to reach a critical value.

Having this in mind, we can proceed and evaluate the expressions needed for the computation of the GSIFs. Assume that $\boldsymbol{\sigma}_0$ and $\boldsymbol{\sigma}_1$ lie in the statically admissible space (see detailed definition in Reference 10), then $\mathscr{B}_c$ and $\mathscr{F}_c$ are given by:

$$\mathscr{B}_c(\boldsymbol{\sigma}_0, \boldsymbol{\sigma}_1) = \int\int_{\Omega_R} \boldsymbol{\sigma}_0^T [E]^{-1} \boldsymbol{\sigma}_1 \, d\Omega \tag{37}$$

$$\mathscr{F}_c(\boldsymbol{\sigma}_1) = \int_{\partial\Omega_R^{(u)}} \hat{\mathbf{u}}^T [A_2] \boldsymbol{\sigma}_1 \, ds \tag{38}$$

where $[E]$ is the material matrix, $[A_2]$ is the matrix given in Reference 1, and $\partial\Omega_R^{(u)}$ is the part of the boundary where the displacement vector $\hat{\mathbf{u}}$ is prescribed.

4.1. *Extraction of the GSIFs using approximated eigenpairs*

The stress tensor is evaluated in terms of the displacement vector given in (36) as follows:

$$\boldsymbol{\sigma} = [E][D]\mathbf{u} \tag{39}$$

$[D]$ is the differential matrix operator given in equation (27) in Reference 1. The 3×1 vector, corresponding to $[D]\mathbf{u}$ will be denoted by $\mathbf{Du}$, and its elements can be explicitly obtained using (36):

$$\begin{aligned}(Du)_1^j = r^{(\alpha_j^{(\mathscr{R})}-1)} \sum_{m=1}^{p+1} & [\cos\theta\cos\delta_j(\alpha_j^{(\mathscr{R})} a_{jm}^{(\mathscr{R})} - \alpha_j^{(\mathscr{I})} a_{jm}^{(\mathscr{I})}) \\ & - \cos\theta\sin\delta_j(\alpha_j^{(\mathscr{R})} a_{jm}^{(\mathscr{I})} + \alpha_j^{(\mathscr{I})} a_{jm}^{(\mathscr{R})})] N_m(\theta(\xi)) \\ & + [-a_{jm}^{(\mathscr{R})}\sin\theta\cos\delta_j + a_{jm}^{(\mathscr{I})}\sin\theta\sin\delta_j] N_m'(\xi)\frac{2}{\omega - \theta_1}\end{aligned} \tag{40}$$

$$\begin{aligned}(Du)_2^j = r^{(\alpha_j^{(\mathscr{R})}-1)} \sum_{m=1}^{p+1} & [\sin\theta\cos\delta_j(\alpha_j^{(\mathscr{R})} b_{jm}^{(\mathscr{R})} - \alpha_j^{(\mathscr{I})} b_{jm}^{(\mathscr{I})}) \\ & - \sin\theta\sin\delta_j(\alpha_j^{(\mathscr{R})} b_{jm}^{(\mathscr{I})} + \alpha_j^{(\mathscr{I})} b_{jm}^{(\mathscr{R})})] N_m(\theta(\xi)) \\ & + [b_{jm}^{(\mathscr{R})}\cos\theta\cos\delta_j - b_{jm}^{(\mathscr{I})}\cos\theta\sin\delta_j] N_m'(\xi)\frac{2}{\omega - \theta_1}\end{aligned} \tag{41}$$

$$
\begin{aligned}
(Du)_3^j = r^{(\alpha_j^{(\mathscr{R})}-1)} \sum_{m=1}^{p+1} & [\sin\theta\cos\delta_j(\alpha_j^{(\mathscr{R})} a_{jm}^{(\mathscr{R})} - \alpha_j^{(\mathscr{I})} a_{jm}^{(\mathscr{I})}) \\
& - \sin\theta\sin\delta_j(\alpha_j^{(\mathscr{R})} a_{jm}^{(\mathscr{I})} + \alpha_j^{(\mathscr{I})} a_{jm}^{(\mathscr{R})}) \\
& + \cos\theta\cos\delta_j(\alpha_j^{(\mathscr{R})} b_{jm}^{(\mathscr{R})} - \alpha_j^{(\mathscr{I})} b_{jm}^{(\mathscr{I})}) \\
& - \cos\theta\sin\delta_j(\alpha_j^{(\mathscr{R})} b_{jm}^{(\mathscr{I})} + \alpha_j^{(\mathscr{I})} b_{jm}^{(\mathscr{R})})] N_m(\theta(\xi)) \\
& + [a_{jm}^{(\mathscr{R})}\cos\theta\cos\delta_j - a_{jm}^{(\mathscr{I})}\cos\theta\sin\delta_j \\
& - b_{jm}^{(\mathscr{R})}\sin\theta\cos\delta_j + b_{jm}^{(\mathscr{I})}\sin\theta\sin\delta_j] N'_m(\xi)\frac{2}{\omega-\theta_1}
\end{aligned} \tag{42}
$$

where $\delta_j \overset{\text{def}}{=} \alpha_j^{(\mathscr{I})} \ln r$, and N_m are the shape functions on an edge. If α_j is complex, then the elements of the $j+1$ vector **Du**, are:

$$
\begin{aligned}
(Du)_1^{j+1} = r^{(\alpha_j^{(\mathscr{R})}-1)} \sum_{m=1}^{p+1} & [\cos\theta\cos\delta_j(\alpha_j^{(\mathscr{R})} a_{jm}^{(\mathscr{I})} + \alpha_j^{(\mathscr{I})} a_{jm}^{(\mathscr{R})}) \\
& + \cos\theta\sin\delta_j(\alpha_j^{(\mathscr{R})} a_{jm}^{(\mathscr{R})} - \alpha_j^{(\mathscr{I})} a_{jm}^{(\mathscr{I})})] N_m(\theta(\xi)) \\
& - [a_{jm}^{(\mathscr{R})}\sin\theta\sin\delta_j + a_{jm}^{(\mathscr{I})}\sin\theta\cos\delta_j] N'_m(\xi)\frac{2}{\omega-\theta_1}
\end{aligned} \tag{43}
$$

$$
\begin{aligned}
(Du)_2^{j+1} = r^{(\alpha_j^{(\mathscr{I})}-1)} \sum_{m=1}^{p+1} & [\sin\theta\cos\delta_j(\alpha_j^{(\mathscr{R})} b_{jm}^{(\mathscr{I})} + \alpha_j^{(\mathscr{I})} b_{jm}^{(\mathscr{R})}) \\
& + \sin\theta\sin\delta_j(\alpha_j^{(\mathscr{R})} b_{jm}^{(\mathscr{R})} - \alpha_j^{(\mathscr{I})} b_{jm}^{(\mathscr{I})})] N_m(\theta(\xi)) \\
& + [b_{jm}^{(\mathscr{R})}\cos\theta\sin\delta_j + b_{jm}^{(\mathscr{I})}\cos\theta\cos\delta_j] N'_m(\xi)\frac{2}{\omega-\theta_1}
\end{aligned} \tag{44}
$$

$$
\begin{aligned}
(Du)_3^{j+1} = r^{(\alpha_j^{(\mathscr{R})}-1)} \sum_{m=1}^{p+1} & [\sin\theta\cos\delta_j(\alpha_j^{(\mathscr{R})} a_{jm}^{(\mathscr{I})} + \alpha_j^{(\mathscr{I})} a_{jm}^{(\mathscr{R})}) \\
& + \sin\theta\sin\delta_j(\alpha_j^{(\mathscr{R})} a_{jm}^{(\mathscr{R})} - \alpha_j^{(\mathscr{I})} a_{jm}^{(\mathscr{I})}) \\
& + \cos\theta\cos\delta_j(\alpha_j^{(\mathscr{R})} b_{jm}^{(\mathscr{I})} + \alpha_j^{(\mathscr{I})} b_{jm}^{(\mathscr{R})}) \\
& + \cos\theta\sin\delta_j(\alpha_j^{(\mathscr{R})} b_{jm}^{(\mathscr{R})} - \alpha_j^{(\mathscr{I})} b_{jm}^{(\mathscr{I})})] N_m(\theta(\xi)) \\
& + [a_{jm}^{(\mathscr{R})}\cos\theta\sin\delta_j + a_{jm}^{(\mathscr{I})}\cos\theta\cos\delta_j \\
& - b_{jm}^{(\mathscr{R})}\sin\theta\sin\delta_j - b_{jm}^{(\mathscr{I})}\sin\theta\cos\delta_j] N'_m(\xi)\frac{2}{\omega-\theta_1}
\end{aligned} \tag{45}
$$

Define $(\tilde{D}u)_k^j \overset{\text{def}}{=} (Du)_k^j/(r^{(\alpha_j^{(\mathscr{I})}-1)})$, so that the ijth term of the compliance matrix which corresponds to the bilinear form is given by

$$
(B_c)_{ji} = \int_0^R \int_{\theta 1}^{\omega} r^{(\alpha_i^{(\mathscr{I})}+\alpha_j^{(\mathscr{I})}-1)} \sum_{l,k=1}^{3} (\tilde{D}u)_k^j E_{kl} (\tilde{D}u)_l^i \, \mathrm{d}r\, \mathrm{d}\theta \tag{46}
$$

The numerical evaluation of the integral (46) requires Gauss quadrature in both the r and θ directions. When comparing to the scalar elliptic problem, where we could reduce the double integration to integration in one dimension only, this integration is less efficient, and we have

$$(B_c)_{ji} = \frac{R}{2} \sum_{l=1}^{n} \frac{\omega^{(l)} - \theta_1^{(l)}}{2} \sum_{q=1}^{N_G} \sum_{s=1}^{N_G} \sum_{\ell,k=1}^{3} W_s W_q r(\eta_s)^{(\alpha_i^{(\omega)} + \alpha_j^{(\omega)} - 1)} (\tilde{D}u)_k^j E_{k\ell}^{(l)} (\tilde{D}u)_\ell^i \tag{47}$$

As previously explained, the stress tensor defined in (39) automatically satisfies the boundary conditions on all boundaries except Γ_R, so that the linear form (38) degenerates to an integral over the circular boundary Γ_R alone. Defining the vector $\hat{\mathbf{u}}_0 \overset{\text{def}}{=} (\hat{u}_x \cos\theta, \hat{u}_y \sin\theta, \hat{u}_x \sin\theta + \hat{u}_y \cos\theta)^T$ (38) becomes

$$\mathscr{F}_c = R \int_{\theta_i}^{\omega} \hat{\mathbf{u}}_0^T [E](\mathbf{Du})|_{(r=R)} \, d\theta \tag{48}$$

The jth term of the load vector corresponding to the linear form can be explicitly computed

$$(F_c)_j = R^{\alpha_j^{(\omega)}} \sum_{l=1}^{n} \frac{\omega^{(l)} - \theta_1^{(l)}}{2} \sum_{q=1}^{N_G} W_q \sum_{\ell,k=1}^{3} (\hat{u}_0)_k (\theta(q)) E_{k\ell}^{(l)} [(\tilde{D}u)_\ell^j]_{r=R} \tag{49}$$

4.2. *Isotropic model problem*

Let us consider the edge-cracked panel in an isotropic material studied by Szabó and Babuška[2]. Plane strain situation and Poisson's ratio of 0·3 were assumed. The first and second GSIFs were computed by the CIM and CFM and it was demonstrated that the rate of convergence using these methods is as fast as the rate of convergence of the strain energy. It should be noted that the exact eigenpairs were used in Reference 2.

To demonstrate the overall numerical method, the approximated eigenpairs obtained by the modified Steklov method were used. These approximated eigenpairs are computed using a 4-element mesh at $p = 6$. The two eigenvalues obtained are $\alpha_1 = 0{\cdot}49999967$, $\alpha_2 = 0{\cdot}50000051$ (the exact values are $\frac{1}{2}$).

The tractions that exactly correspond to the stresses of Mode 1 and Mode 2 stress fields were applied on the boundaries of the solution domain chosen to be defined exactly as in Reference 2, with same finite element mesh. See Figure 8. We select the first two GSIFs to be A (A is arbitrary) and defined the normalized stress intensity factors $\tilde{A}_1$ and $\tilde{A}_2$ as follows:

$$\tilde{A}_i \overset{\text{def}}{=} (A_i)_{FE}/A, \quad i = 1, 2 \tag{50}$$

In this way both normalized GSIFs have to converge to 1 as the number of degrees of freedom is increased.

The first two normalized GSIFs are extracted taking R to be 0·5. The number of degrees of freedom, the error in energy norm, and the computed values of the normalized GSIFs are listed in Table III. The relative error in the energy norm, the relative error in the strain energy, and the absolute value of the relative error in the first GSIF, computed by our method and by the CIM, are plotted against the number of degrees of freedom on a log–log scale in Figure 9. The same data for the second GSIF is shown in Figure 10.

It is seen that the rate of convergence of the GSIFs is faster than the rate of convergence of the solution measured in energy norm and both the CIM and our method have similar convergence patterns. As the error in energy norm decreases the CIM (based on the exact eigenpairs) performs

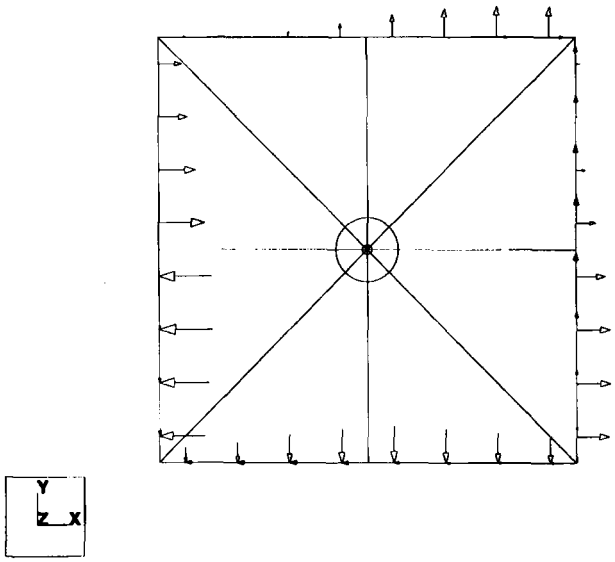

Figure 8. Solution domain and mesh design for a crack in an isotropic material

Table III. The first two GSIFs for a crack in an isotropic material

	$p=1$	$p=2$	$p=3$	$p=4$	$p=5$	$p=6$	$p=7$	$p=8$
DOF	53	155	273	439	653	915	1225	1583
$\|e\|_E(\%)$	29·92	11·07	5·52	3·15	2·24	1·78	1·48	1·26
$\tilde{A}_1$	0·8144	0·9548	0·9912	0·99783	0·99795	0·99825	0·99862	0·99882
$\tilde{A}_2$	0·8317	0·9641	0·9946	0·99942	0·99888	0·99898	0·99926	0·99943

better than our method (based on the approximated eigenpairs). However, up to the relative error of approximately 0·1 per cent the performance of both methods is virtually the same.

This example problem demonstrates the efficiency of the proposed extraction method when applied to isotropic materials.

4.3. Crack at a bimaterial interface

A bimaterial is a composite of two homogeneous materials, with continuity of tractions and displacements across interfaces maintained. When the materials are isotropic, a closed form solution for the stress tensor can be obtained using Muskhelishvili's[15] methods. Referring to Figure 11, we define

$$\varepsilon = \frac{1}{2\pi} \ln\left(\frac{\kappa_1 \mu_2 + \mu_1}{\kappa_2 \mu_1 + \mu_2}\right) \tag{51}$$

where

$$\kappa = \begin{cases} 3 - 4\nu & \text{for plane strain} \\ (3 - \nu)/(1 + \nu) & \text{for plane stress} \end{cases}$$

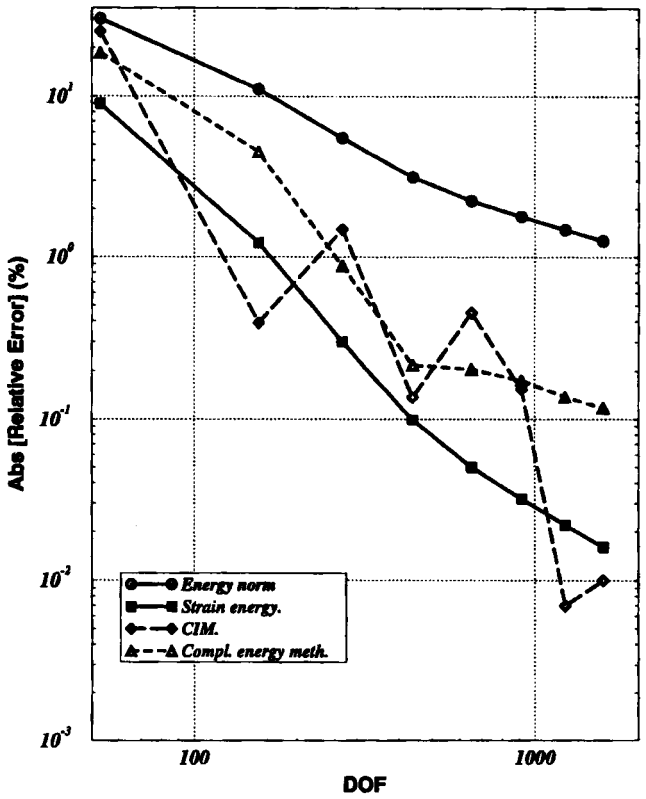

Figure 9. Convergence of $\|e\|_E$, the strain energy ($\|e\|_E^2$), and A_1 for a crack in an isotropic material

and μ is the shear modulus. Following Suo,[16†] and ignoring terms which remain bounded at the crack tip, the asymptotic stress fields in material 1 can be put into the form:

$$\sigma_{ij} = \frac{1}{\sqrt{2\pi r}} \{K_I[\cos(\varepsilon \ln r)\,\sigma_{ij}^{\Re} + \sin(\varepsilon \ln r)\,\sigma_{ij}^{\Im}] + K_{II}[-\sin(\varepsilon \ln r)\,\sigma_{ij}^{\Re} + \cos(\varepsilon \ln r)\,\sigma_{ij}^{\Im}]\} \quad i,j = r,\theta \tag{52}$$

where

$$\begin{aligned}
\sigma_{rr}^{\Re} &= [-\sinh \varepsilon(\pi-\theta)\cos(\tfrac{3}{2}\theta) + e^{-\varepsilon(\pi-\theta)}\cos(\tfrac{1}{2}\theta)(1+\sin^2(\tfrac{1}{2}\theta) + \varepsilon\sin(\theta))]/\cosh \varepsilon\pi \\
\sigma_{\theta\theta}^{\Re} &= [\sinh \varepsilon(\pi-\theta)\cos(\tfrac{3}{2}\theta) + e^{-\varepsilon(\pi-\theta)}\cos(\tfrac{1}{2}\theta)(\cos^2(\tfrac{1}{2}\theta) - \varepsilon\sin(\theta))]/\cosh \varepsilon\pi \\
\sigma_{r\theta}^{\Re} &= [\sinh \varepsilon(\pi-\theta)\sin(\tfrac{3}{2}\theta) + e^{-\varepsilon(\pi-\theta)}\sin(\tfrac{1}{2}\theta)(\cos^2(\tfrac{1}{2}\theta) - \varepsilon\sin(\theta))]/\cosh \varepsilon\pi \\
\sigma_{rr}^{\Im} &= [\cosh \varepsilon(\pi-\theta)\sin(\tfrac{3}{2}\theta) - e^{-\varepsilon(\pi-\theta)}\sin(\tfrac{1}{2}\theta)(1+\cos^2(\tfrac{1}{2}\theta) - \varepsilon\sin(\theta))]/\cosh \varepsilon\pi \\
\sigma_{\theta\theta}^{\Im} &= [-\cosh \varepsilon(\pi-\theta)\sin(\tfrac{3}{2}\theta) - e^{-\varepsilon(\pi-\theta)}\sin(\tfrac{1}{2}\theta)(\sin^2(\tfrac{1}{2}\theta) + \varepsilon\sin(\theta))]/\cosh \varepsilon\pi \\
\sigma_{r\theta}^{\Im} &= [\cosh \varepsilon(\pi-\theta)\cos(\tfrac{3}{2}\theta) + e^{-\varepsilon(\pi-\theta)}\cos(\tfrac{1}{2}\theta)(\sin^2(\tfrac{1}{2}\theta) + \varepsilon\sin(\theta))]/\cosh \varepsilon\pi
\end{aligned} \tag{53}$$

† The expressions for the displacements in Reference 16 are not continuous across the interface at $\theta = 0$, therefore could not possibly be valid

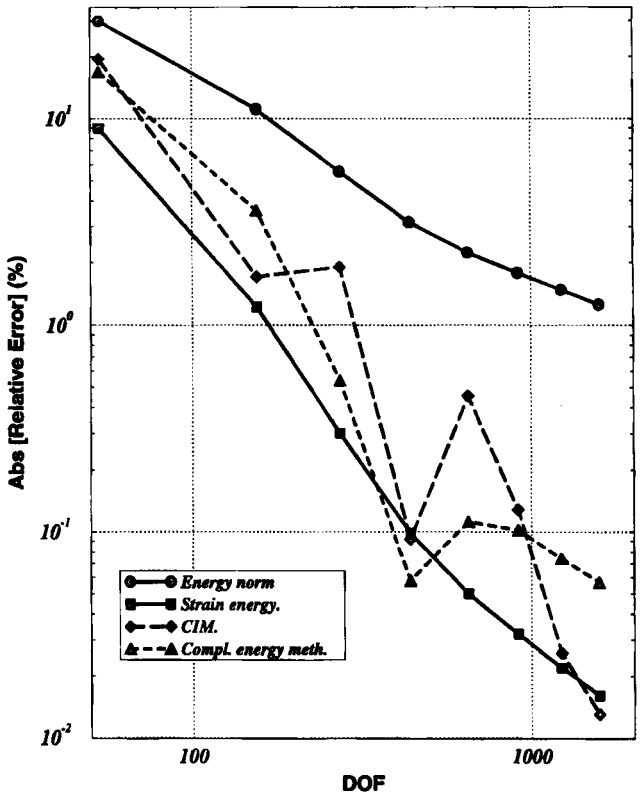

Figure 10. Convergence of $\|e\|_E$, the strain energy ($\|e\|_E^2$), and A_2 for a crack in an isotropic material

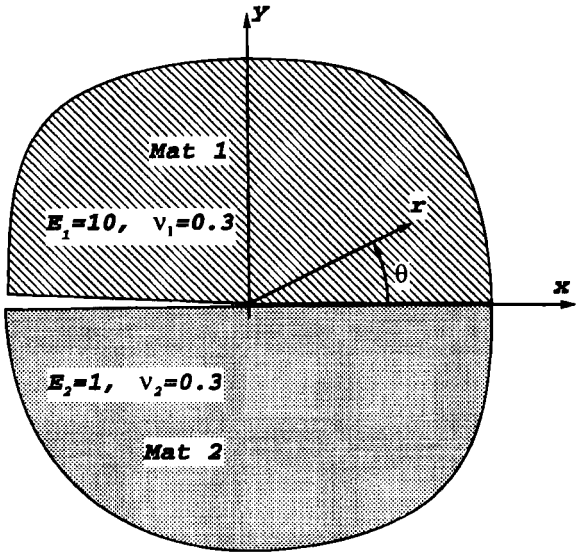

Figure 11. Crack at a bimaterial interface example problem

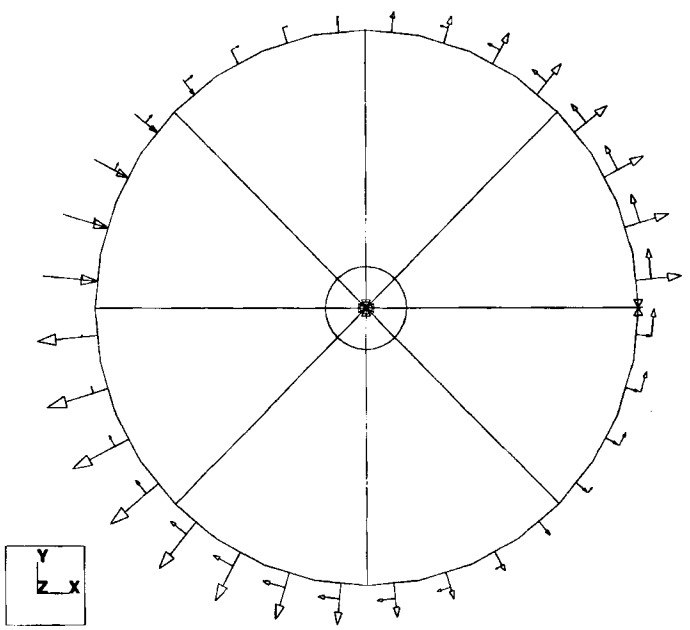

Figure 12. Solution domain and mesh design for a crack at a bimaterial interface

The stress fields in material 2 can be obtained by replacing the combination $\varepsilon\pi$ to $-\varepsilon\pi$ everywhere in (54). The first eigenvalue for this crack problem is complex and is given by $\frac{1}{2} \pm i\varepsilon$. Analytic methods for the computation of the stress intensity factors are available only for some simple geometries and loadings. Because of the complexity of these methods, numerical procedures are a necessity.

An early numerical method for extracting stress intensity factors (SIFs) for cracks along bimaterial interfaces from finite element solutions is given in Reference 17, where a special hybrid crack tip finite element was used. Hong *et al.*[18] used the contour integral method for bimaterial interfaces. Although these methods provide good results, they require complicated computational procedures, have to be tailored to a specific finite element code, cannot analyse anisotropic materials and are restricted to specific geometries. Smelser[19] used the crack flank displacement data for extracting the SIFs, however, the reported data have low accuracy. All of these methods require the knowledge of the exact eigenpairs, and are strictly restricted to a particular geometry.

The accuracy and convergence behaviour of our method is demonstrated on the bimaterial fracture mechanics problem shown in Figure 11 where plane strain situation is assumed. The exact eigenpairs are utilized in equation (37). As suggested in the previous model problem, the tractions that exactly correspond to the singular stress field in (52) were applied on the sides of a circular solution domain shown in Figure 12. The outer radius of the domain has the radius of 1·5 and the two refined layers around the singular point have the radii $0{\cdot}15 \times 1{\cdot}5$ and $0{\cdot}15^2 \times 1{\cdot}5$. The polynomial level of the trial and test functions is increased over the shown mesh from 1 to 8. The stress intensity factors K_I and K_{II} in the expressions for the applied tractions are arbitrarily selected to be K. Again, we define the normalized stress intensity factors $\tilde{K}_I$ and $\tilde{K}_{II}$ analogously to (50) and expect that the extracted values for the $\tilde{K}$s will converge to 1 as the number of degrees of freedom is increased.

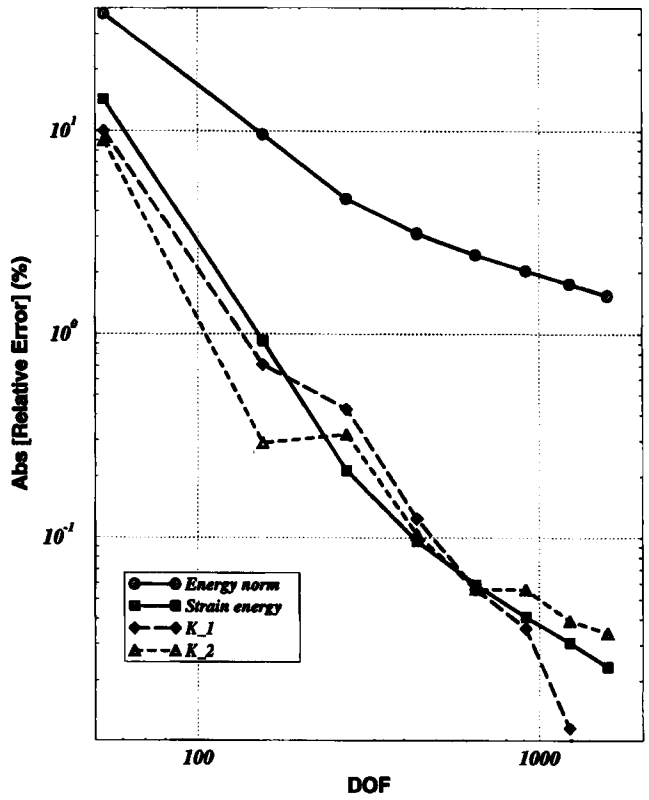

Figure 13. Convergence of $\|e\|_E$, the strain energy ($\|e\|_E^2$), and the errors in $\bar{K}_I$ and $\bar{K}_{II}$ for a crack at a bimaterial interface

Figure 13 shows the relative error in the energy norm, the relative error in strain energy and the absolute value of the relative error in the extracted SIFs as the number of degrees of freedom is increased on a log–log scale. The computations were done using an integration radius of 1·3. It is seen, as in the case of an isotropic material, that the existence of complex eigenpairs has no influence on the performance of the proposed method, and the SIFs converge to the exact values virtually as fast as the convergence rate of the strain energy. This example demonstrates that an accurate and efficient numerical solution of fracture mechanics problems, even for such complicated situations as the crack at a bimaterial interface, is possible. Additionally, the method is equally well suited for any other singular point, without further changes.

5. SUMMARY AND CONCLUSIONS

The computation of engineering data from finite element solutions of two-dimensional linear elliptic boundary value problems of second order was investigated. The principal objective was to develop efficient and reliable methods for the computation of the coefficients of asymptotic expansions in the vicinity of singular points, called generalized flux intensity factors (GFIFs) and generalized stress intensity factors (GSIFs). A key requirement was that the methods must be applicable to anisotropic and heterogeneous materials. The reason for this requirement is that investigation of failure initiation events in composite materials involves the key parameters that

characterize the solutions in the vicinity of singular points. Another important requirement was that the method developed in a two-dimensional setting has to be extendible to three dimensions.

The investigation addressed two important areas: (a) the characterization of the solution by means of eigenfunctions in the vicinity of singular points, which was reported in Reference 1 and (b) extraction of the key parameters from the finite element solution.

A new indirect method for extracting the GFIFs/GSIFs and first derivatives from the finite element solution, based on the complementary weak form was developed. This new *superconvergent* method was formulated and analysed in detail on the basis of the Laplace problem in two dimensions in Reference 9. Mathematical analysis, followed by numerical examples, demonstrated the efficiency and accuracy of the results.

It was shown theoretically that the computed values converge to the exact ones at least as fast as the energy norm. It was demonstrated numerically that the convergence is as fast as the energy norm squared, that is the strain energy.

The proposed method has five major advantages: (a) The error in the pointwise data of interest exhibits superconvergence. (b) The method is general in the sense that it is applicable to any point of the domain using the same algorithm. (c) The method is applicable to anisotropic materials, and any type of singularities, including those associated with multi-material interfaces. (d) The method can be used in conjunction with any finite element analysis program. (e) The method is extendible to three-dimensional problems.

The formulation and numerical examples for the anisotropic scalar problem, as well as for the elasticity problem, are provided. It is demonstrated that the general behaviour of the extracted values is very similar to that observed for the Laplace problem.

ACKNOWLEDGEMENTS

The support of this work by the Air Force Office of Scientific Research under grant No. F49620-93-1-0173 is gratefully acknowledged.

REFERENCES

1. Z. Yosibash, B. A. Szabó, 'Numerical analysis of singularities in two dimensions. Part 1: Computation of eigenpairs', *Int. j. numer. methods eng.*, **38**, 2055–2082 (1995).
2. B. A. Szabó and I. Babuška, 'Computation of the amplitude of stress singular terms for cracks and reentrant corners', in T. A. Cruse (ed.), *Fracture Mechanics: 19th Symp.*, ASTM STP 969, ASTM, Philadelphia, 1988, pp. 101–124.
3. Z. Yosibash and B. Schiff, 'A superelement for two-dimensional singular boundary value problem in linear elasticity', *Int. J. Fract.*, **62**(4), 325–340 (1993).
4. I. Babuška and A. Miller, 'The post processing approach in the finite element method—part 2: The calculation of stress intensity factors', *Int. j. numer. methods eng.*, **20**, 1111–1129 (1984).
5. L. Banks-Sills and D. Sherman, 'Comparison of methods for calculating stress intensity factors with quarter-point elements', *Int. j. Fract.*, **32**, 127–140 (1986).
6. I. Babuška, T. Von-Petersdorff and B. Andersson, 'Numerical treatment of vertex singularities and intensity factors for mixed boundary value problems for the Laplace equation in $\mathbb{R}^3$', *SIAM J. Numer. Anal.*, **31**, 1265–1288 (1994).
7. P. Grisvard, *Elliptic Problems in Nonsmooth Domains*, Pitman, London 1985.
8. I. Babuška, and M. Suri, 'The *p*- and *h*–*p* versions of the finite element method—An overview', *Comput. Methods Appl. Mech. Eng*; **80**, 5–26 (1990).
9. B. A. Szabó and Z. Yosibash, 'Superconvergent extraction of flux intensity factors and first derivatives from finite element solutions', *Comput. Methods Appl. Mech. Eng.*, in press.
10. B. A. Szabó and I. Babuška, *Finite Element Analysis*, Wiley, New York 1991.
11. Z. Yosibash, 'Numerical analysis of singularities and first derivatives for elliptic boundary value problems in two dimensions', *D.Sc. dissertation*, Sever Institute of Technology, Washington University, St. Louis, MO, U.S.A, August 1994.
12. M. L. Williams, 'The stresses around a fault or crack in dissimilar media', *Bull. Seismol. Soc. Am.*, **49**, 199–204 (1959).
13. J. R. Rice and G. C. Sih, 'Plane problems of cracks in dissimilar media', *Trans. ASME, J. Appl. Mech.*, **32**, 418–423 (1965).

14. A. H. England, 'A crack between dissimilar media', *Trans. ASME, J. Appl. Mech.*, **32**, 400–402 (1965).
15. N. I. Muskhelishvili, *Some Basic Problems of the Mathematical Theory of Elasticity*, Noordhoff, Leiden, 1953.
16. Z. Suo, Mechanics of interface fracture, *Ph.D. dissertation*, Harvard University, Cambridge, MA, U.S.A., May 1989.
17. K. Y. Lin and J. W. Mar, 'Finite element analysis of stress intensity factors for cracks at a bi-material interface', *Int. J. Fract.*, **12**, 521–531 (1976).
18. C. Hong and M. Stern, 'The computation of stress intensity factors in dissimilar materials', *J. Elasticity*, **8**, 21–34 (1978).
19. R. E. Smelser, 'Evaluation of stress intensity factors for bimaterial bodies using numerical flank displacement data', *Int. J. Fract.*, **15**, 135–143 (1979).